ANALYSIS OF ATMOSPHERIC WATER VAPOR MAPS FROM AVIRIS AT SALTON SEA, CALIFORNIA: PART II, SURFACE MOISTURE FLUX, BOUNDARY CONDITIONS, AND PLUME MEASUREMENTS

James E. Conel and Veronique Carrere

Jet Propulsion Laboratory
California Institute of Technology
Pasadena, California

ABSTRACT

Several applications of AVIRIS water vapor imagery to problems of land surface evaporation, velocity determinations in the atmospheric water vapor boundary layer, and studies of fetch requirements and boundary conditions on turbulent diffusion models are described in a preliminary way, using elementary results from atmospheric diffusion theory. A search for water vapor plumes from a geothermal power plant cooling tower is reported, together with calculations on plume dimensions expected for the atmospheric stability conditions and source strength.

INTRODUCTION

Part I of this study reported progress on application of the continuum integrated band ratio (CIBR) method to mapping of atmospheric water vapor over the Salton Sea test site. The experimental goals were described, and random and systematic errors that lead to uncertainties in the water determinations and discrepancies between amounts retrieved using different bands were enumerated. The importance of atmospheric scattering was emphasized, both from the standpoint of dependence of the calibration curves on visibility and upon choice of the scattering model, e.g., rural vs marine aerosol models, both of which among others are resident in the LOWTRAN 7 code. The dependence of retrievals upon departures of the actual surface reflectance from the wavelength-independent value assumed in construction of CIBR calibration curves was also described.

In this paper we describe some applications using elementary results of the theory of atmospheric diffusion of the AVIRIS-derived water maps. In so doing we acknowledge the probable poor accuracy of the water vapor determinations used, and instead exploit the relatively good precision. The problem of land surface evaporation is investigated from the standpoint of the atmospheric water budget method (Brutsaert, 1982). The conservation equation for atmospheric moisture can be arranged, using the divergence theorem of Gauss, to provide surface flux over a region in terms of the moisture advected normally across the enclosing vertical boundaries. This leads to tentative consideration of how to determine horizontal velocity in the water vapor boundary layer using water vapor as a tracer. A second investigation deals with fetch requirements for the observed column abundances and boundary conditions on an atmospheric turbulent diffusion model, using the onshore distribution of moisture as a result of sea-breeze circulation. Finally, we describe a search for the water vapor plume from the cooling tower of a geothermal plant located at the southern end of the Salton Sea. The amount of moisture emitted from this source is known; hence

it may form a useful example for pollution or volcanic source strength evaluation using AVIRIS images.

LAND SURFACE MOISTURE FLUXES AND SURFACE BOUNDARY CONDITIONS

Evaporation from land and water surfaces represents an important component of the hydrologic cycle and constitutes the connection between the surface water budget and the energy budget (Brutsaert, 1982, 1986). Utilization of AVIRIS spectral data allows routine mapping of column abundance distributions. Separation of the total amount thus observed into components from local evaporation or evapotranspiration sources versus components advected into a scene across the vertical boundaries surrounding it is a fundamental problem. In an earlier paper (Conel, et al., 1989) we explored models of the atmospheric moisture distribution arising across abrupt changes in surface conditions, e.g., between wet and dry areas, under steady winds (Sutton's problem, Sutton, 1953: Brutsaert, 1982). Our analyses pointed out characteristics of the spatial variation of the column abundance with respect to the assumed surface boundary condition discontinuity that might lead to identification of the nature of the surface boundary conditions and to estimation of fluxes from the surface.

Here, we explore the feasibility of using AVIRIS data for such investigations. The present discussion amplifies on use of time sequences of AVIRIS images to estimate surface evaporation. We also present an example from data over the western shore at Salton Sea that may represent a plume from the lake developed in response to a steady onshore sea breeze.

A strategy for recovery of surface moisture flux from time sequences of AVIRIS observations. The equation of conservation for atmospheric water vapor (Brutsaert, 1982) can be written, neglecting horizontal gradients of the turbulent fluxes as well as molecular diffusion,

$$\frac{\partial \overline{q}}{\partial t} + \frac{\partial}{\partial x}(\overline{u}\overline{q}) + \frac{\partial}{\partial y}(\overline{v}\overline{q}) + \frac{\partial}{\partial z}(\overline{w}\overline{q}) = -\frac{\partial}{\partial z}(\overline{w'q'}) + S_v \qquad (1)$$

where $\overline{q}$ is the specific humidity, $\overline{u}$,$\overline{v}$, and $\overline{w}$ are mean velocities in directions x, y, and z (x, y, horizontal, and z vertical), w' is the turbulent velocity fluctuation in the z-direction, $\overline{q}'$ is the turbulent fluctuation of specific humidity, and S_v is a source term representing the difference between vaporization and condensation at a point in grams of water per gram of moist air per unit time. AVIRIS observations provide estimates of the column abundance W of precipitable water, e.g.,

$$W = \int_0^\infty \overline{q}\rho dz \qquad (2)$$

where ρ is the density of moist air, taken to be the mean standard value in the boundary layer. The integral extends from the surface to the top of the atmosphere, which we assume to be 20 km, the flight altitude of AVIRIS.

Integrating Equation 2 over z in this fashion, with $\overline{w}\overline{q}$ equal to zero at the surface and top of the atmosphere and $\overline{w}$,$\overline{q}$, also zero at the top, gives

$$\frac{\partial W}{\partial t} + \nabla \cdot \int_0^\infty (U\bar{q})\rho dz = E - P \qquad (3)$$

where $U = i\bar{u} + j\bar{v}$ and i and j are unit vectors in the x and y directions, respectively. In addition, $E = \rho \overline{w'q'}$ is the evaporation flux at the surface and $P = -\int_0^\infty S_v \rho dz$ is the loss of moisture from condensation throughout the column. Forming areal averages over a scene by multiplying both sides of Equation 3 by dA/A and integrating gives

$$\frac{\partial \bar{W}}{\partial t} + \frac{1}{A}\int_0^\infty \int_S (\bar{q}U_n)\rho dS dz = \bar{E} - \bar{P} \qquad (4)$$

where use has also been made of the divergence theorem to convert the volume integral of Equation 3 to a surface integral in Equation 4 extending over vertical boundaries of the volume enclosing the scene. In Equation 4, $\bar{W}$, $\bar{E}$, and $\bar{P}$ denote spatial average values and U_n is the component of the wind normal to S, positive outward. Assuming winds $\bar{u}(z)$ parallel to the x axis blowing in the + x direction, and averages over a strip $0 \leq x \leq L$ and unit width in the y direction, Equation 4 written out becomes

$$\frac{\partial \bar{W}}{\partial t} + \frac{1}{L}\left[-\int_0^\infty \overline{uq}\rho dz \,\Big|_{x=0} + \int_0^\infty \overline{uq}\rho dz \,\Big|_{x=L} \right] = \bar{E} - \bar{P} \qquad (5)$$

In Equations 3, 4, and 5, the long-term time averages $\langle \partial W/\partial t \rangle$ and $\langle \partial \bar{W}/\partial t \rangle$ are much smaller than the other terms so averaged, and are therefore negligible (Peixoto and Oort, 1983; Kinter and Shukla, 1990). This mathematical simplification, however, does not appear to have associated practical consequences, since accumulation of the requisite AVIRIS data sets is not feasible. For example, we examined a series of 484 column precipitable water abundances (W), derived from rawinsonde observations at Edwards AFB, California for the period March 1988 through April 1989, and found a roughly cyclic variation throughout the period. An accumulation of several years of such observations would appear to be required to estimate the long-term mean and variance with any assurance. Further analysis of this problem is under way.

The further evaluation of Equation 5 leading to a determination of $\bar{E}$ for the scene (assuming precipitation $\bar{P}$ to be zero for the observational period) requires measurement of $\bar{u}$ and $\bar{q}$ with altitude along the boundaries, together with $\partial \bar{W}/\partial t$.

Aircraft measurements of moisture flux rely on limited stacks of flight lines over some boundaries, together with measurements with onboard sensors of vertical velocity and humidity fluctuations averaged over the flight paths (e.g., Betts, *et al.*, 1990; Desjardins, *et al.*, 1989). Restricted sample time and sampling length through the air impose limitations on accuracy of such flux retrievals (Lenschow and Stankov, 1986). The duration of sampling flights over Kansas during the FIFE project was on the order of two hours (Betts, *et al.*, 1990). Such aircraft measurements have led to underestimates of the sensible and latent heat fluxes at the surface compared to values from surface stations (Betts, *et al.*, 1990).

With AVIRIS, large areal sampling (swath width = 11 km) of column abundance occurs rapidly (e.g., 1/12 second per line, representing a strip 20 m in width on the ground perpendicular to the flight direction). But direct observations of wind speed and specific humidity with altitude are not available. Rather, it appears necessary to proceed indirectly by first seeking to recover average wind speed from changes in moisture patterns in time sequences of observations. Such time sequences are feasible in practice with AVIRIS at intervals of about 15 minutes.

The mean wind speed $d\bar{X}/dt$ (Pasquill and Smith, 1983, sec 3.3; also called the local convective velocity by Csanady (1973)) is given by

$$\frac{d\bar{X}}{dt} = \frac{1}{W}\int_0^\infty \overline{uq}\rho dz \qquad (6)$$

so that the integral $\int_0^\infty \overline{uq}\rho dz$ could be estimated at a point if a value of $d\bar{X}/dt$ were available. Since $\bar{X}$ represents the mean horizontal displacement of an ensemble of moisture "particles," it might be feasible to map changes in mean position of features in W with time, thereby employing the water vapor column abundance fluctuations as a wind tracer. An alternative and probably superior strategy would be to examine the cross correlations between time sequences of moisture profiles to determine the lag for maximum correlation between features present as a measure of displacement over the time interval between measurements. This is the method employed by Eloranta, *et al.* (1975) to determine wind speed in the boundary layer, using lidar, to observe drift of features in the aerosol backscatter.

Evaluation of $d\bar{X}/dt$ for power law profiles of $\bar{u}(z)$ and K(z) and steady-state conditions. To get an idea of the magnitude of $d\bar{X}/dt$ and its relation to specific vertical wind u(z) and eddy diffusivity K(z) profiles, we work out Equation 6 for the steady-state case of evaporation from a uniformly moist surface of width L with specific humidity $\bar{q}(0)$ (at $z = 0$) $= \bar{q}_0$ in $0 \leqq x \leqq L$, surrounded by dry land areas with $q(0) = 0$, $x < 0$, and $x > L$. The wind speed and eddy diffusivity are $\bar{u}(z) = az^m$, $K(z) = bz^n$. The solution for $\bar{q}$ in $0 < x < L$, $z > 0$ (Brutsaert, 1982, ch. 7) is

$$\bar{q}(\upsilon,\xi) = \bar{q}_0\,[1 - P(\upsilon,\xi)] \qquad (7)$$

where $P(\upsilon,\xi)$ is the incomplete gamma function, $\upsilon = (1 - n)/(2 + m - n)$, and

$$\xi = \frac{a}{b(2 + m - n)^2}\,\frac{z^{2 + m - n}}{x} \qquad (8)$$

The integrals for W from Equation 2 and the product of $\overline{uq}$ over z in Equation 6 can be evaluated (Abramowitz and Stegun, 1964) to give

$$\frac{d\bar{X}}{dt} = a\left[\left(\frac{b}{a}\right)(2 + m - n)^2 x\right]^{\upsilon}\left[(m + 1)\Gamma\left(\frac{2 - n}{2 + m - n}\right)\right]^{-1} \qquad (9)$$

where $\Gamma(c)$ is the gamma function. Adopting the values of $m = 1/7$ and $n = 1 - m$, (e.g., Brutsaert, 1982, ch. 4) gives $d\bar{X}/dt = 0.86a(b/a)^{1/9}x^{1/9}$. Thus the apparent average speed increases with x (although weakly), even though $\bar{u}(z)$ is independent of horizontal distance. The $x^{1/9}$ dependence of $d\bar{X}/dt$ arises as a consequence of the continuity condition (Equation 8). The total

evaporative moisture crossing $x = \eta$ from advection is equal to $\int_0^\eta E(x)dx$, which is proportional to $\eta^{8/9}$. The column abundance W is proportional to $\eta^{7/9}$.

The constants a and b in Equation 14 are given by

$$a = \bar{u}_1/z_1^m \qquad \text{and} \qquad b \cong u_*^2/(ma) \tag{10}$$

(Brutsaert, 1982, ch. 4 and p. 160). In Equation 10, $\bar{u}_1$ is the mean wind speed at height z_1 above the surface, and u_* is the friction velocity, a quantity that depends upon surface roughness. Typical values for u_* range from 0.16 m/s for a smooth surface such as mud or ice to 0.63 m/s for long grass (Sutton, 1953, p. 233). Adopting $u_* = 0.3$ m/s and $\bar{u}_1 = 2$ m/s at a height of 2 m gives $d\bar{X}/dt = 1.87x^{1/9}$, where x is in meters. For example at $x = 10^4$ m, the apparent speed is 5.2 m/s as compared to an apparent speed of 1.9 m/s at x = 1 m.

If the wind speed and eddy diffusivity are constant with altitude, i.e., m and n equal to zero in Equation 9, $d\bar{X}/dt = a$, the assumed value of $\bar{u}$.

The quantity $d\bar{X}/dt$ calculated in this example cannot ordinarily be observed. The moisture distribution is steady, and no features within it move relative to the surface. Evaluation of the average speed under such conditions would require actual measurements of $\bar{u}(z)$, K(z), and W. Under ordinary conditions, however, water vapor distributions can be expected to contain irregularities. An important question relates to the expected lifetime under atmospheric diffusion processes of any given irregularity, compared to the minimum observation time interval achievable with AVIRIS (about 10 minutes).

Time scale for dispersion of irregularities in the water distribution compared to minimum interval of atmospheric observations with AVIRIS. To estimate the time scale for dispersion of irregularities in the moisture distribution as observed by AVIRIS, we have used a simple puff diffusion model, the formulas for which are readily available (Seinfeld, 1986; Hanna, *et al.*, 1982). A puff is thought of as an instantaneous release at a point, whereas any real irregularity, however it might have been generated, would presumably evolve over a finite period of time and with finite spatial dimensions. On this basis more realistic models could be evolved by evaluating the Lagrangian equation for the mean concentration (Seinfeld, 1986, p. 561), taking account of both finite source size and finite emission time; but for the present it seems adequate to provide estimates from the simpler instantaneous point-source model. The Gaussian puff formula, including total reflection of water vapor at the surface (i.e., no losses there) for a source at the point $x = y = 0$ at time $t = 0$ and integrated out over vertical distance z to correspond to the column abundance, can be derived from a formula given by Seinfeld (1986, p 570) by application of Equation 2 to give

$$W_{puff}(x,y) = \frac{S}{2\pi\sigma_x\sigma_y}\exp\left[-\frac{(x - \bar{u}t)^2}{2\sigma_x^2} - \frac{y^2}{2\sigma_y^2}\right] \tag{11}$$

where S is the source strength in grams. If the pixel size of AVIRIS is of length and width l, then the abundance over a pixel at the origin is

$$\bar{W}_{puff} = S \, \mathrm{erf}\left(\frac{l}{2\sqrt{(2)}\sigma_y}\right) \mathrm{erf}\left(\frac{l/2 - \bar{u}t}{2\sqrt{(2)}\sigma_x}\right) \qquad (12)$$

For σ_x and σ_y (= σ), we use estimates obtained from fits of the graphical data given by Hanna, *et al.* (1982, p. 43), which yield $\sigma \cong 0.1t$, where σ is in m and t in s. Using these values, a pixel size of 20 m and an AVIRIS observation repeat time of 15 minutes yields the relative degradation in the y direction to be proportional to erf(0.094), or about 10% of the original puff strength. After one-half hour the relative strength is reduced to erf(0.047), or about 5% of the original value. Changes in the x direction could be similarly evaluated by translating the integration area with the maximum in the distribution, which is found at $x = \bar{u}t$ at any time t. The possible recurrence observation time for the relative decay of fluctuations at the 10% level is thus about equivalent to the feasible recurrence observation time interval with AVIRIS.

FETCH REQUIREMENTS AND BOUNDARY CONDITIONS

Nature of the analysis. We analyzed a segment of the northeast-southwest AVIRIS flight line over the western shore (Figure 1/Slide 12) to look for characteristic changes in atmospheric moisture distribution inland that might be identified with specific forms of the surface boundary conditions on the atmospheric turbulent diffusion problem. In this section we examine the constant-surface-humidity source model for Salton Sea and the zero-surface-humidity condition for the onshore region. Are the observed moisture abundances consistent with dimensions of the source region, and is the pattern of moisture variation onshore consistent with other physical circumstances of the problem, e.g., the implied moisture flux at the surface for maintenance of a zero surface concentration there? A difficulty with these preliminary calculations is that no satisfactory estimate of background moisture abundance is available. Therefore the amounts of water we are seeking to generate by the fetch, temperature, and wind conditions, or dispose of by the boundary conditions, or lose by topographic variation, are too great. The present calculations therefore represent extremes of variation that would probably be reduced once the background is properly assessed.

Water distribution images for the western shore segment. The atmospheric precipitable water distribution observed for the western shore segment of the NE-SW AVIRIS line at Salton Sea (see Figure 2 of paper I for location of the western shore segment), and computed using the 940-nm water band, is given in Figure 1b. It is compared there with a three-color composite image of the area, with the band color designations red = 651 nm, green = 552 nm, blue = 454 nm, as indicated in Figure 1a. The water distribution image shows a residual herringbone pattern of coherent noise, but depicts a well defined falloff in water abundance traversing inland left to right, parallel to the onshore wind direction (compare with Figure 5, paper I). The onshore profile of column moisture variation between points A and B in Figure 1b is shown in Figure 2.

Atmospheric moisture distribution for constant-specific-humidity boundary conditions. Analytically simple conditions are constant-specific humidity (m,n non zero) or constant moisture flux (m,n = 0). Conel *et al.* (1989) worked out expressions for column abundance changes across discontinuities in surface conditions involving wet and dry surfaces for both types of boundary conditions, assuming constant wind speed and diffusivity (m = n = 0) and no change in roughness between regions. Here we confine attention to the surface humidity boundary condition. Specifically, for the boundary value problem leading to Equation 7, the specific humidity $\bar{q}$ is

$$\bar{q}(v,\xi,\xi_1) = \bar{q}_0[P(v,\xi_1) - P(v,\xi)] \qquad (x > L) \quad (13)$$

with ξ given by Equation 8 and ξ_1 by Equation 8 with x replaced by x − L. The corresponding column abundance W is obtained from Equation 2:

$$W(x,m,n) = \rho\bar{q}_0 \frac{\Gamma\left(\frac{2-n}{2+m-n}\right)}{\Gamma\left(\frac{1-n}{2+m-n}\right)}\left[\left(\frac{b}{a}\right)(2+m-n)^2\right]^{1/(2+m-n)}\left[x^{1/(2+m-n)} - (x-L)^{1/(2+m-n)}\right] \qquad (x > L) \quad (14)$$

$$W(x,0,0) = \rho\bar{q}_0 \frac{2}{\sqrt{\pi}}\left(\frac{b}{a}\right)^{1/2}\left[x^{1/2} - (x-L)^{1/2}\right] \qquad (x > L) \quad (15)$$

and

$$W(x,1/7,6/7) = \rho\bar{q}_0 \frac{\Gamma(8/9)}{\Gamma(1/9)}\left(\frac{9}{7}\right)^{14/9}\left(\frac{b}{a}\right)^{7/9}\left[x^{7/9} - (x-L)^{7/9}\right] \qquad (x>L) \quad (16)$$

Fetch requirement for on-shore column abundance on the constant-surface-humidity model. Are the AVIRIS-derived column abundances for the western shore segment consistent with origin of the column moisture as evaporation and transport via horizontal advection from Salton Sea under the constant-surface-humidity model? The total column abundance W(L,m,n) at the shoreline x = L in Equation 13 provides an estimate of the fetch L over Salton Sea required to generate the observed total moisture present in the column at the shore. From this expression, using the notation L(m,n) to designate the fetch for given indices m and n,

$$L(0,0) = \frac{\pi}{4}\left(\frac{a}{b}\right)\left(\frac{W(L,0,0)^2}{\rho^2\bar{q}_0^2}\right) \quad (17)$$

and

$$L(1/7,6/7) = \left(\frac{7}{9}\right)^2\left(\frac{a}{b}\right)\left[\frac{W(L,1/7,6/7)\Gamma(1/9)}{\rho\bar{q}_0\,\Gamma(8/9)}\right]^{9/7} \quad (18)$$

Using Equation 10, and adopting values of a = 200 cm/s, z_1 = 200 cm, b_0 = 10^5 cm^2/s (see Seinfeld, 1986, p. 598) and $u_* = 30$ cm/s, $\rho = 1.18\times10^{-3}$ g/cm^3 for the density of dry air at a temperature of 300K and $\bar{q}_0 = 2.16\times10^{-2}$ g water/g air for the saturation concentration at that temperature, gives L(0,0) = 65 km and L(1/7,6/7) = 180 km ($\Gamma(1/9) = 8.523$, $\Gamma(8/9) = 1.078$).

Conversely, if L = 10 km, with these same values, $W(L,0,0) = 0.64$ g/cm^2 and $W(L,1/7,6/7) = 0.172$ g/cm^2.

The fetches implied for the observed shoreline column abundances on these models are thus much greater than the actual dimensions of Salton Sea in the direction of the surface winds. The discrepancies may be greater when the actual wind field generated by the lake is accounted for. For example, a theoretical study of lake and land breezes generated by diurnal heating over small (circular) lakes (Neumann and Mahrer, 1975) shows the lake breezes to be strongly divergent horizontally and zero in speed at the center. Thus, in addition to violation of the constant-with-x horizontal wind speed assumption, the available fetch is only one-half the actual width of the water body. The total onshore column abundance observed at x = L in the profile may therefore be comprised of a component of water surface origin that is advected by the breeze, and a resident background component that is inherited from other sources. It may be thought possible to estimate such a background component by identifying it with the moisture amount in equilibrium with the lake under zero wind conditions. However, from Equations 10 and 14, W(x,m,n) is undefined with a = 0 in the simple diffusion model employed here.

Estimation of column abundance variation due to topography. The moisture profile given in Figure 2 contains some variation from decrease of moisture with elevation. The elevation difference is about 70 m over the 11.6-km length of the profile. The actual variation of water vapor concentration with height at the western shore site is not known. We estimated the expected falloff for the 70-m rise from the water vapor distribution resident in the LOWTRAN 7 default midlatitude summer atmospheric model. The vertical water vapor concentration $\bar{c}(z)$ (in g cm^{-2}km^{-1}) over the first 10 km, which contains nearly all of the moisture present in the model, can be represented accurately by two exponential distributions of the form $\bar{c}_j(z) = A_j \exp(-\beta_j z)$, j = 1,2, where j = 1 applies over $0 < z < 2$ km , and j = 2 over $2 < z < 10$ km. From the model, $A_1 = 1.372$, and $A_2 = 1.772$, and $\beta_1 = 0.54$, and $\beta_2 = 0.68$. The A_j factor can be eliminated by expressing $W(z)$, the vertically integrated water vapor above any altitude z in terms of W_A, the observed shoreline column abundance, and by assuming continuity in the distribution at z = 2 km. The expression for W(z) between $0 < z < 2$ km scaled in this way is

$$W(z) = W_A\left[\int_z^2 \bar{c}_1(\zeta)d\zeta + \exp(-\beta_1 \cdot 2)\int_2^{10} \bar{c}_2(\zeta)d\zeta\right] \times\left[\int_0^2 \bar{c}_1(\zeta)d\zeta + \exp(-\beta_1 \cdot 2)\int_2^{10} \bar{c}_2(\zeta)d\zeta\right]^{-1} \quad (19)$$

The observed distribution, together with the expected variation from the topographic rise calculated according to Equation 19, and the difference, or anomalous water variation, are plotted in Figure 3. The observed distribution plotted here represents a smoothed (average) version of that given in full in Figure 2.

Comparison of residual or anomalous profile with profiles expected from atmospheric diffusion models with concentration boundary conditions. The expected variation of atmospheric moisture along the inland traverse in Figure 2, according to the diffusion model with constant concentration

boundary conditions, was calculated according to the formula

$$W'(L,x',m,n) = \frac{W'(0,m,n)}{L^{1/(2+m-n)}}\left[(x' + L)^{1/(2+m-n)} - (x')^{1/(2+m-n)}\right] \quad (20)$$
$$(x' > L)$$

where the obvious transformation $x' = x - L$ has been used. The fetch L is defined by equations 17 and 18 in terms of the observed precipitable water at $x' = 0$, the upstream ($x < L$) values of ρ and $\bar{q}_0$, and adopted constants a and b (or b_0). Equation 20 is compared in Figure 4 with the anomalous distribution, i.e., that distribution obtained after correction for topography according to the LOWTRAN model.

Surface flux implied by onshore falloff in moisture on the constant-surface-humidity model. An instructive test of the zero surface-specific humidity condition is provided by the implied flux of moisture into the surface required by the falloff in anomalous atmospheric moisture abundance inland. The flux f_0 of moisture at the surface for $x > L$ is

$$f_0 = -K(z)\frac{\partial \bar{q}_0}{\partial z}\bigg|_{z=0} = -\frac{b\bar{q}_o\rho}{\Gamma(\upsilon)}\left[\left(\frac{a}{b}\right)\frac{1}{(2 + m - n)^2}\right]^{\upsilon} \quad (21)$$
$$\times\left[\left(\frac{1}{x - L}\right)^{\upsilon} - \left(\frac{1}{x}\right)^{\upsilon}\right](2 + m - n)$$

where L is given by Equation 17 or 18 in terms of the measured column abundance at $x = L$ and the adopted values of ρ and $\bar{q}_0$ over $0 < x < L$. Surface fluxes for the two models $m = n = 0$ and $m = 1/7$, $n = 6/7$ are plotted in Figure 5. Maintenance of the condition $\bar{q}_0(x,0) = 0$ requires the continuous absorption of large amounts of water by the surface, which would seemingly, sooner or later, be manifested as surface runoff. These conditions were not observed at the surface near the shore, nor elsewhere inland. Thus the observed column abundance variation depicted in Figures 1 and 2 cannot reasonably arise as a simple manifestation of the concentration boundary conditions assumed in the diffusion model.

Vertical distribution of moisture implied by column abundance variation over topography in a laterally homogeneous atmosphere. An alternative interpretation of the moisture profile variation given in Figure 2 is that the changes result dominantly from the topographic variation and therefore in some sense reflect the actual variation of atmospheric moisture vertically at the time of observation. For a laterally homogeneous atmosphere (i.e., $\bar{q}(x,z) = \bar{q}_h(z)$) without influence of advection or eddy diffusion, the column abundance W(x) above any surface elevation $z_s = z_s(x)$ with $z_s = 0$ as local Salton Sea level, is

$$W(x) = \int_{z_s(x)}^{\infty} \rho\bar{q}_h(\zeta)d\zeta \quad (22)$$

Thus $dW(x)/dx = -\rho\bar{q}_h(z_s)(dz_s/dx)$, and the slope of the column abundance variation yields $\bar{q}_h(z_s)$, provided dz_s/dx is known. Conversely, for zero advection/diffusion conditions, i.e., a horizontally layered atmosphere, extraction of land surface slope based on the slope of the column abundance variation requires knowledge of the local column abundance, the density

being given. The moisture concentration $\bar{c}_h(z) = \rho\bar{q}_h(z)$ in g/cm^2km, derived from dW/dx for the onshore profile, is given in Figure 6.

CONSEQUENCES OF A HORIZONTALLY VARYING ADVECTION VELOCITY

Results of the previous two sections show that the observed onshore declining column moisture abundance probably does not arise as a consequence of topographic variation and cannot arise as a consequence of a flux of moisture into the surface implied by zero-specific humidity at z = 0. Up to this point nothing has been said about the likely complex distribution of moisture and wind velocity over the sea and inland that would accompany the sea breeze circulation. The sea breeze associated with diurnal heating of "small" lakes (25 to 50 km in radius) and their surroundings has been investigated by Neumann and Mahrer (1974). The actual distribution of moisture in cross section in sea breeze circulation was measured considerably earlier by Craig, et al. (1945). Neumann and Mahrer (1974) calculated that the land breezes are horizontally divergent. As heating progresses, cool air penetrates landward along a front whose position is 10 to 20 km inland from the shoreline. The frontal zone is characterized by convergence of the horizontal wind at low altitude and upward motion on and immediately ahead of the front. Above a near-surface zone approximately 600 meters thick, countercirculation is present with winds blowing lakeward. Such flows and counterflows have been observed in smoke patterns along the shore of Lake Michigan at Chicago (Lyons and Olsson, 1973). The model calculations (Neumann and Mahrer, 1975) also indicate uplift of isotherms ahead of the front and downward indentation behind it that accompany the heating cycle. Similar patterns were expected in the vertical and horizontal distributions of water vapor, which, in fact, appeared in the measurements of atmospheric humidity reported by Craig *et al.* (1945), cited earlier here.

We want to exploit the simple, nearly constant divergence of the horizontal velocity near shore implied by these model calculations over both sea and land to compute the expected horizontal variation of the column abundance. Steady flow conditions are assumed and confined to the (x,z) plane. The topography is neglected. (See footnote (†) below for a scheme to include topography.) The horizontal velocity is taken independent of z and to vary with x according to

$$\bar{u}(x,z) = \bar{u}_0 + \alpha x \tag{23}$$

where $\bar{u}_0$ is the value of $\bar{u}$ at $x = x_0$, and α is the divergence of the horizontal velocity. The condition of incompressibility yields for the vertical velocity $\bar{w}$

$$\bar{w}(x,z) = - \alpha z \tag{24}$$

Integrating Equation 1 vertically using Equation 2, the column abundance W(x,z) obeys

$$(\bar{u}_0 + \alpha x)\frac{dW}{dx} + \alpha W = f_0 \tag{25}$$

This equation has the solution

$$W(x) = \frac{1}{\bar{u}_0 + \alpha x}\left[(\bar{u}_0 + \alpha x)W(x_0) + \int_{x_0}^{x} f_0(\psi)d\psi\right] \qquad (26)$$

where $W(x_0)$ is the value of W at $x = x_0$.(†)

Equation 26 was fitted to the topographically corrected (anomalous) variation of W given in Figure 4 under the assumption $f_0 = 0$, with $x_0 = 10$ km, $\bar{u}_0 = 200$ cm/s and $\alpha = 2.8 \times 10^{-5}$ s^{-1}. This value of α is consistent with values obtained by Neumann and Mahrer (1974) for small lakes, i.e., 10^{-4} to 10^{-5} s^{-1}.

SEARCH FOR WATER VAPOR PLUMES

A potential application for AVIRIS's capability to provide detailed spatial (and temporal) mapping of the atmosphere is that of inventorying atmospheric constituents. Pollutant assessment and surveying volcanic effluents are two problems of current interest. The identification of plumes in the column abundance distribution would lead immediately to source emission strength by a numerical integration over plume area. We sought to carry out a material balance experiment of this kind for water vapor emission from cooling evaporators and flash towers (Figure 7/Slide 13) at a geothermal power facility located along the southern shore (UNOCAL Salton Sea Unit 3, U3 in Figure 8/Slide 11 of Part I). The total loss of water vapor from such facilities, of which there are six in the area, is monitored hourly. In principle these data, under favorable atmospheric circumstances, can be compared with total abundances derived from the AVIRIS water maps. Before attempting such an assessment, we needed to identify plumes in the AVIRIS water images. To aid this search, simple calculations were made of expected plume dimensions under the known source strength. For simplicity we have assumed in the following that emission is from a point source, although the evaporators and flash tower cover finite dimensions and are physically separated from one another.

The so-called Gaussian plume equation expresses the mean concentration of a species emitted from a continuous, elevated point source. The Gaussian plume formula under the slender plume approximation for mean concentration $\langle c(x,y,z)\rangle$ from a source at height h above the surface, total reflection at the boundary, steady horizontal mean winds $\bar{u} = (\bar{u}, 0, 0)$, and source strength Q (gm sec^{-1}) is (Seinfeld, 1986, Ch 14 and p. 571)

(†) If topographic effects were to be included in the form of a gentle uniform slope, this would introduce a vertical velocity at z = 0 given approximately by $\bar{w}_0(x) = \bar{u}(x)(dz_s/dx)$ [see Smith, 1979, p. 96]. With dz_s/dx unequal to zero, Equation 23 is replaced by $\bar{w} = \bar{w}_0(x) - \alpha z$. The right-hand side of Equation 25 is replaced by $f_0(x) + \bar{w}_0 \rho \bar{q}(x,0)$, with the integral in Equation 26 modified accordingly. To specify $\bar{q}(x,0)$ we might, as an approximation, assume the condition of zero surface flux over the land, i.e., $f_0 = 0$, $x > L$, in which case $\bar{q}(x,0) = 2F_0(b/a)^{1/2}[\sqrt{x} - \sqrt{(x - L)}]/(\sqrt{(\pi)}\rho b)$(Conel, et al., 1989), where F_0 is the water vapor flux at the surface over the water body between $0 \leqq x \leqq L$.

$$\langle c(x,y,z)\rangle = \frac{Q}{2\pi\bar{u}\sigma_y\sigma_z}\exp\left(-\frac{y^2}{2\sigma_y^2}\right)\left[\exp\left(-\frac{(z-h)^2}{2\sigma_z^2}\right)+\exp\left(-\frac{(z+h)^2}{2\sigma_z^2}\right)\right] \quad (27)$$

where $\langle c(x,y,z)\rangle$ is in g/cm^3. In this equation, σ_y and σ_z are the horizontal and vertical dispersion coefficients (in cm) along the y and z axes. The column abundance W is

$$W(x,y) = \frac{1}{\sqrt{(2\pi)}}\frac{Q}{\bar{u}\sigma_y}\exp\left(-\frac{y^2}{2\sigma_y^2}\right) \quad (28)$$

and independent of the source height and the vertical dispersion coefficient σ_z. The total evaporation rate for UNOCAL 3 over a 4-hour time period centered around the time of AVIRIS overflight is nearly steady and is given in Figure 9. (These data were generously supplied by UNOCAL, Indio, California). In addition, we took $\sigma_y(x) = \exp[I_y + J_y \ln x + K_y(\ln x)^2]$ (Seinfeld, 1986, p. 576), where the coefficients I_y, J_y, and K_y are determined by stability class, taken to be Pasquill Class A for the extant conditions of bright sun and ~ 1 m/s^{-1} wind speed. The distribution W(x,y) is plotted in Figure 10, where the size of one AVIRIS pixel (20 × 20 m) is given for comparison. The anomalous water content contributed by the plume, exceeding 0.1 cm in amount, is only about four pixels in length and two in width, even for a source of the magnitude dealt with here (about 75,000 gal/hr). The actual plume dimensions might be expected to exceed this somewhat because of finite source size, but the source magnitude per unit area would correspondingly be reduced. For an AVIRIS detection sensitivity of 0.1 cm, i.e., 10% at 1 pr cm water vapor, the calculated plume area is only a few pixels in size.

Inspection of the column abundance distribution map of Figure 8 discloses no obvious oblong anomaly that might be indentified as the sought-after cloud. This may result from any or all of the following causes: (1) relatively modest detection levels possible from this particular AVIRIS data set, (2) low-speed variable wind conditions, and (3) heavy spatially variable background of water vapor from other multiple sources in the area, including the sea, transpiration from fields, and other power plant emissions. The UNOCAL 3 evaporators apparently contribute to the atmosphere amounts of water comparable to natural sources present in the area. For example, evapotranspiration of 0.65 cm (0.25 in.) of water from agricultural sources (not unreasonable for Imperial Valley conditions) yield about 1.7×10^6 gallons of water vapor per square km. This amount would be supplied to the atmosphere in about 22 hours from the UNOCAL Unit 3 source.

ACKNOWLEDGMENTS

Jack Margolis pointed out the work of Eloranta et al. (1975) and the potential usefulness of their method for measurement of wind speed in the boundary layer using water vapor instead of the aerosol distribution as a tracer. We had many valuable discussions with Carol Bruegge, Rob Green, and Gordon Hoover, all of JPL, and Prof. Fred Share of California State University Long Beach. David G. Newell, Area Production Engineer, UNOCAL Geothermal Division, Indio, California, very kindly supplied the evaporation data for the Salton Sea Unit 3 plant.

This paper presents the results of one phase of research carried out at the Jet Propulsion Laboratory, California Institute of Technology, under a contract with the National Aeronautics and Space Administration.

REFERENCES

Abramowitz, M., and I.A. Stegun, 1964, *Handbook of Mathematical Functions*, National Bureau of Standards Applied Mathematics Series, 55, p. 263.

Betts, A.K., R.L. Desjardins, J.I. MacPherson, and R.D. Kelly, 1990, Boundary-layer heat and moisture budgets from FIFE, *Boundary-Layer Meteorology*, 50, 109-137.

Brutsaert, W., 1982, *Evaporation into the Atmosphere*, D. Reidel Publishing Company, Boston, 299 pp.

Brutsaert, W., 1986, Catchment-scale evaporation and the atmospheric boundary layer, *American Geophysical Union*, Paper No. 5W0661, 39S-45S.

Conel, J.E., R.O. Green, V. Carrere, J.S. Margolis, G.Vane, C. Bruegge, and R.E. Alley, 1989, Spectroscopic measurement of atmospheric water vapor and schemes for determination of evaporation from land and water surfaces using the Airborne Visible/Infrared Imaging Spectrometer (AVIRIS), *IGARSS '89, 12th Candadian Symposium on Remote Sensing*, IEEE #89CH2768-0, 2658-2663.

Craig, R.A., I. Katz, and P.J. Harney, 1945, Sea breeze cross sections from phychrometric measurements, *Bull. Am. Meteor. Soc.*, 26, 405-410.

Csanady, G.T., 1973, *Turbulent diffusion in the environment*, D.Reidel Publishing Co., Dordrecht, 248 pp.

Desjardins, R.L., J.I. MacPherson, P.H. Schuepp, and F. Karanja, 1989, An evaluation of aircraft flux measurements of CO_2, water vapor, and sensible heat, *Boundary-Layer Meteorology*, 47, 55-69.

Eloranta, E.W., J.M. King, and J.A. Weinman, 1975, The determination of wind speed in the boundary layer by monostatic lidar, *J. Appl. Meterol.*, 14, 1485-1489.

Hanna, S.R., G.A. Briggs, and R.P. Hosker, Jr., 1982, *Handbook on Atmospheric Diffusion*, U.S. Department of Energy Document DOE/TIC - 11223, 102 pp.

Kinter, J.L., and J. Shukla, 1990, The global hydrologic and energy cycles: suggestions for studies in the pre-Global Energy and Water Cycle EXperiment (GEWEX), *Bulletin American Meteorological Society*, 71(2), 181-190.

Lenschow, D.H., and B.B. Stankov, 1986, Length scales in the convective boundary layer, *J. Atmos. Sci.*, 43(12), 1198-1209.

Lyons, W.A., and L.E. Olsson, 1973, Detailed mesometeorological studies of air pollution dispersion in the Chicago lake breeze, *Mon. Wea. Rev.*,101(5), 387-403.

Neumann, J., and Y. Mahrer, 1975, A theoretical study of the lake and land breezes of circular lakes, *Mon. Wea. Rev.*, 103, 474-485.

Pasquill, F., and F.B. Smith, 1983, *Atmospheric Diffusion, 3rd Ed.*, Ellis Horwood Limited, Chichester, 436 pp.

Peixoto, J.P., and A.H. Oort, 1983, The atmospheric branch of the hydrological cycle and climate, in *Variations in the Global Water Budget*, (A. Stree-Perrott, M. Beran, and R. Ratcliffe, eds.), D. Reidel Publishing Company, Dordrecht, 5-65.

Seinfeld, J.H., 1986, *Atmospheric physics and chemistry of air pollution*, John Wiley and Sons, New York, 738 pp.

Smith, R.B., 1979, The influence of mountains on the atmosphere, *Advances in Geophysics (B. Saltzman, Ed.)*, 21, 87-230.

Sutton, O.G., 1953, *Micrometeorology*, McGraw-Hill Book Company, New York, 334.

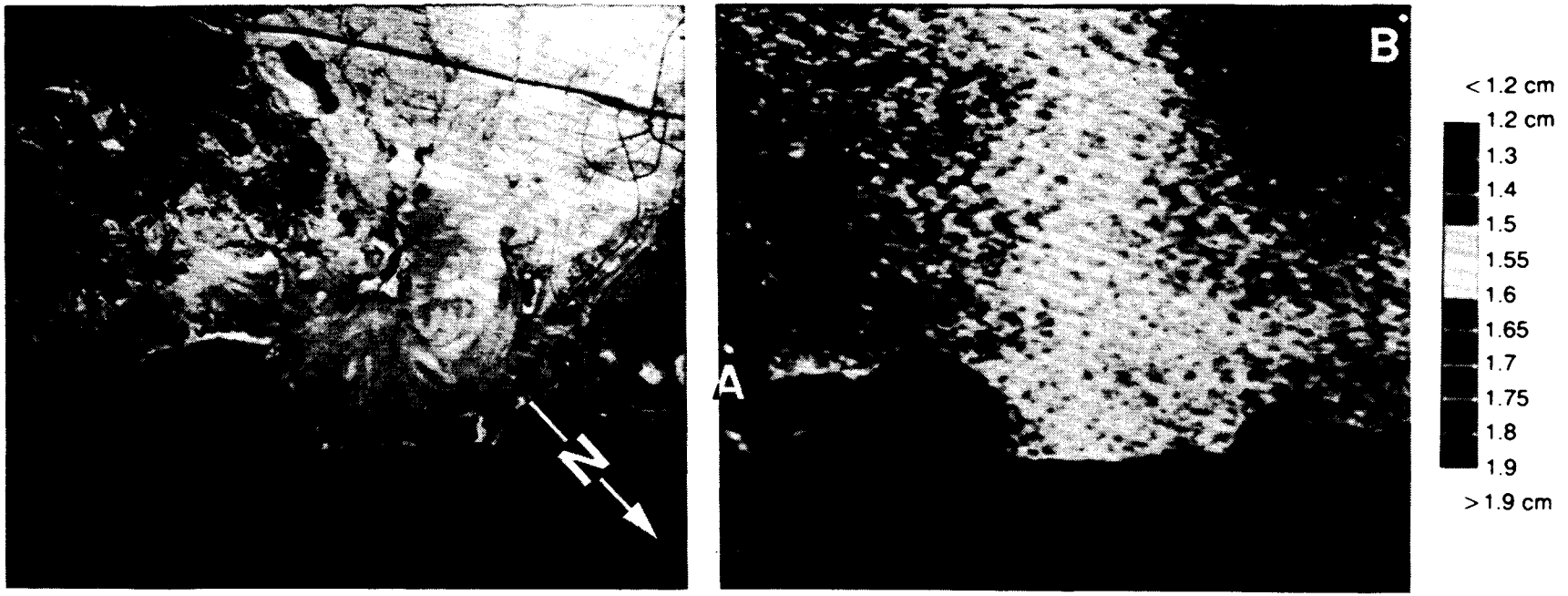

(a) Red: 651 nm Green: 552 nm Blue: 454 nm

(b) Spatial distribution of water vapor
940 nm Atmospheric water band

Figure 1. The 10:50 PST segment of AVIRIS data from the NE-SW flight line at Salton Sea, April 18. 1989. Left panel: three-color composite image. Right panel: distribution of water vapor retrieved for the scene using the continuum interpolated band ratio (CIBR) algorithm described in Part I. The points A and B are ends of the water vapor column abundance profile given in Figure 2. THe AVIRIS image is approximately 11 km in width.

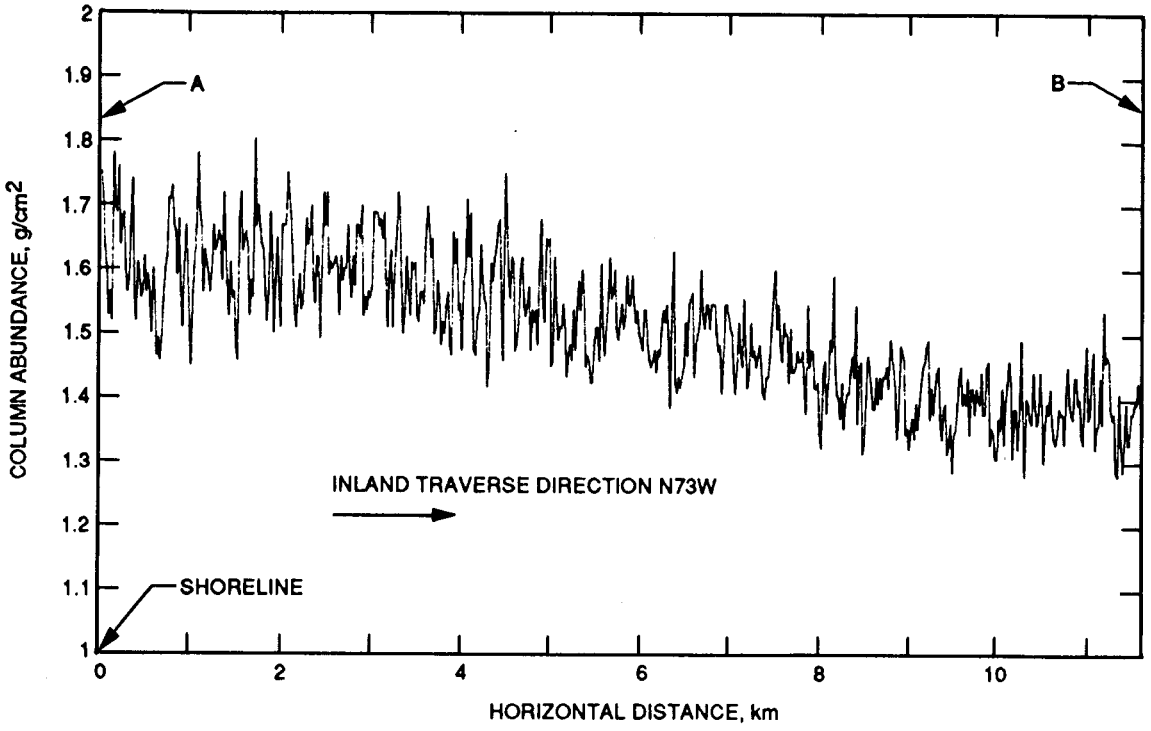

Figure 2. Variation of column moisture abundance along the profile direction AB in Figure 1.

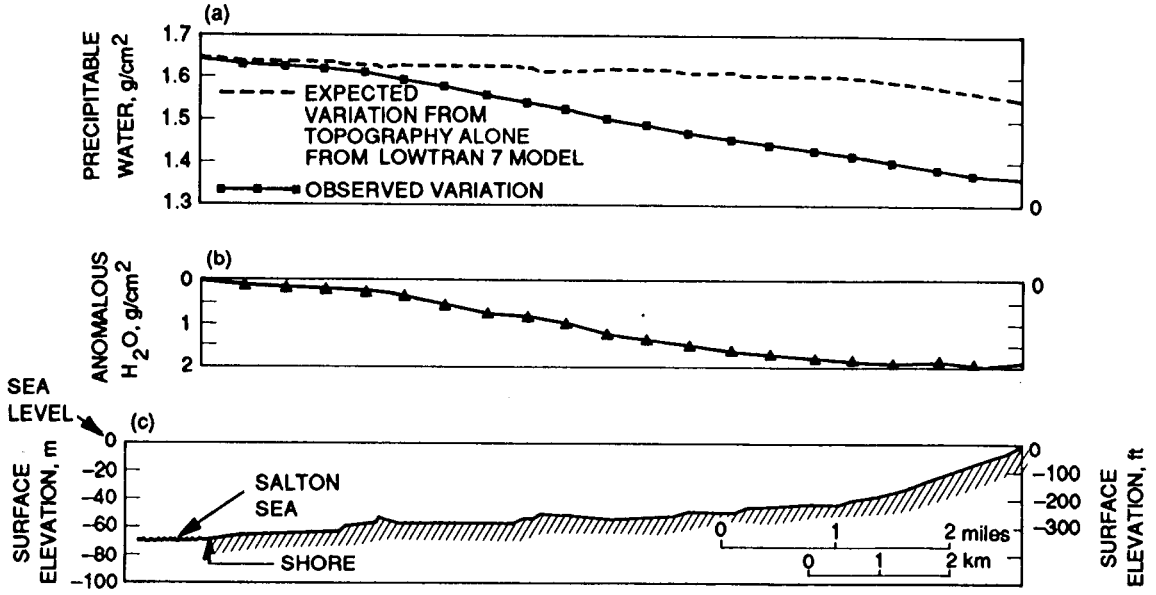

Figure 3. (a) Variation of column moisture abundance along profile AB expected from the vertical moisture concentration in the LOWTRAN 7 mid-latitude summer model together with the observed variation from Figure 2; (b) The *anomalous* column moisture variation obtained as the difference between observed and LOWTRAN 7 distributions; (c) topographic profile along AB.

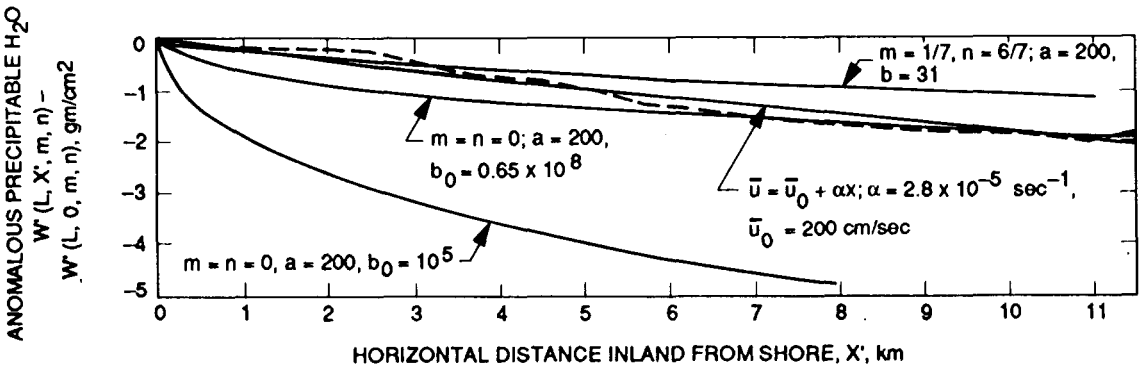

Figure 4. Anomalous moisture profile along AB compared to column abundance variations predicted by an atmospheric diffusion model. The parameters m, n, a, and b describe variation of horizontal velocity and eddy diffusivity with height according to Equation 10.

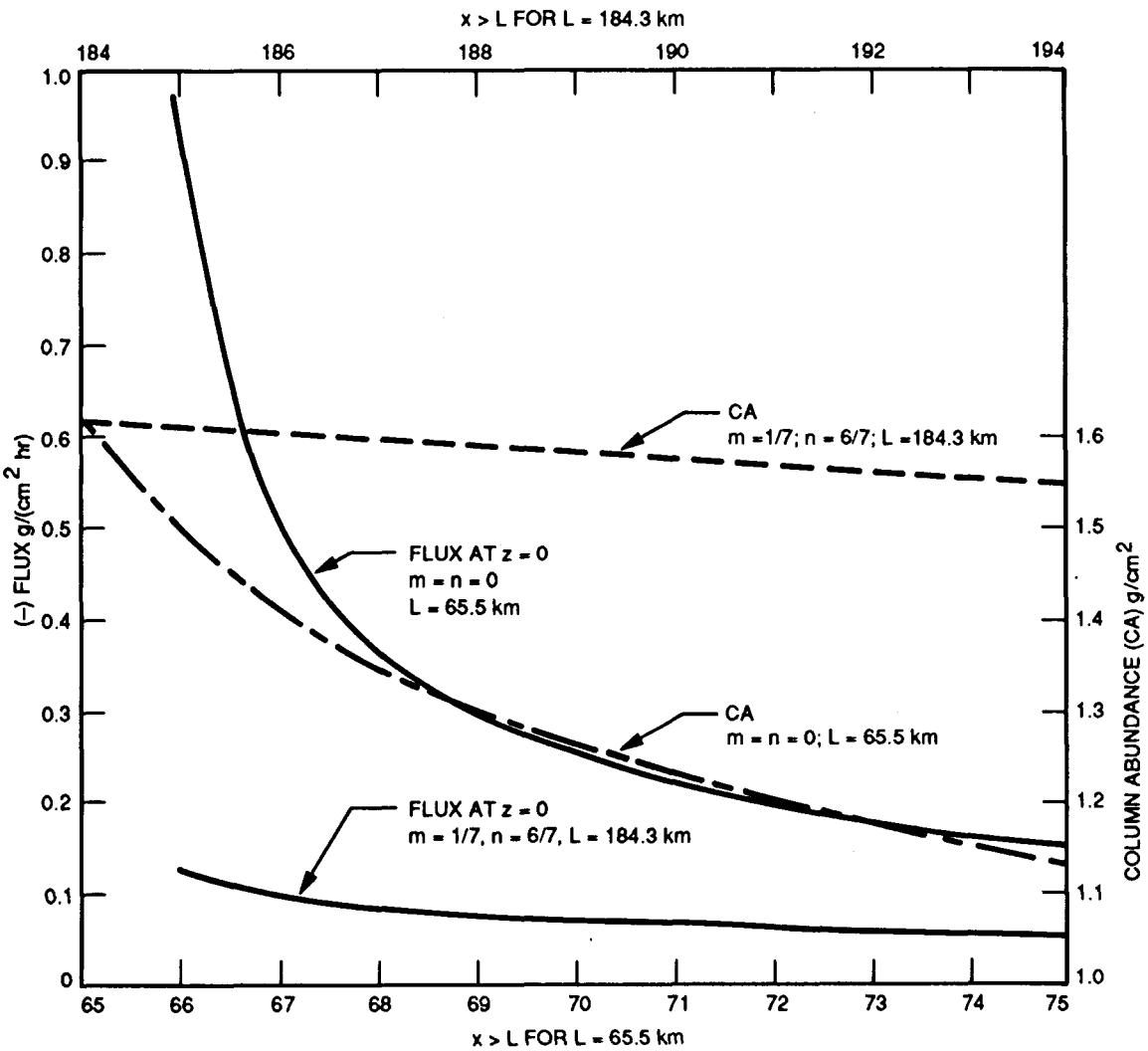

Figure 5. The moisture flux (FLUX) into the surface in g/(cm^{2}hr) and the column abundance variation (CA) implied by the anomalous moisture variation under the inland zero surface-specific humidity boundary condition.

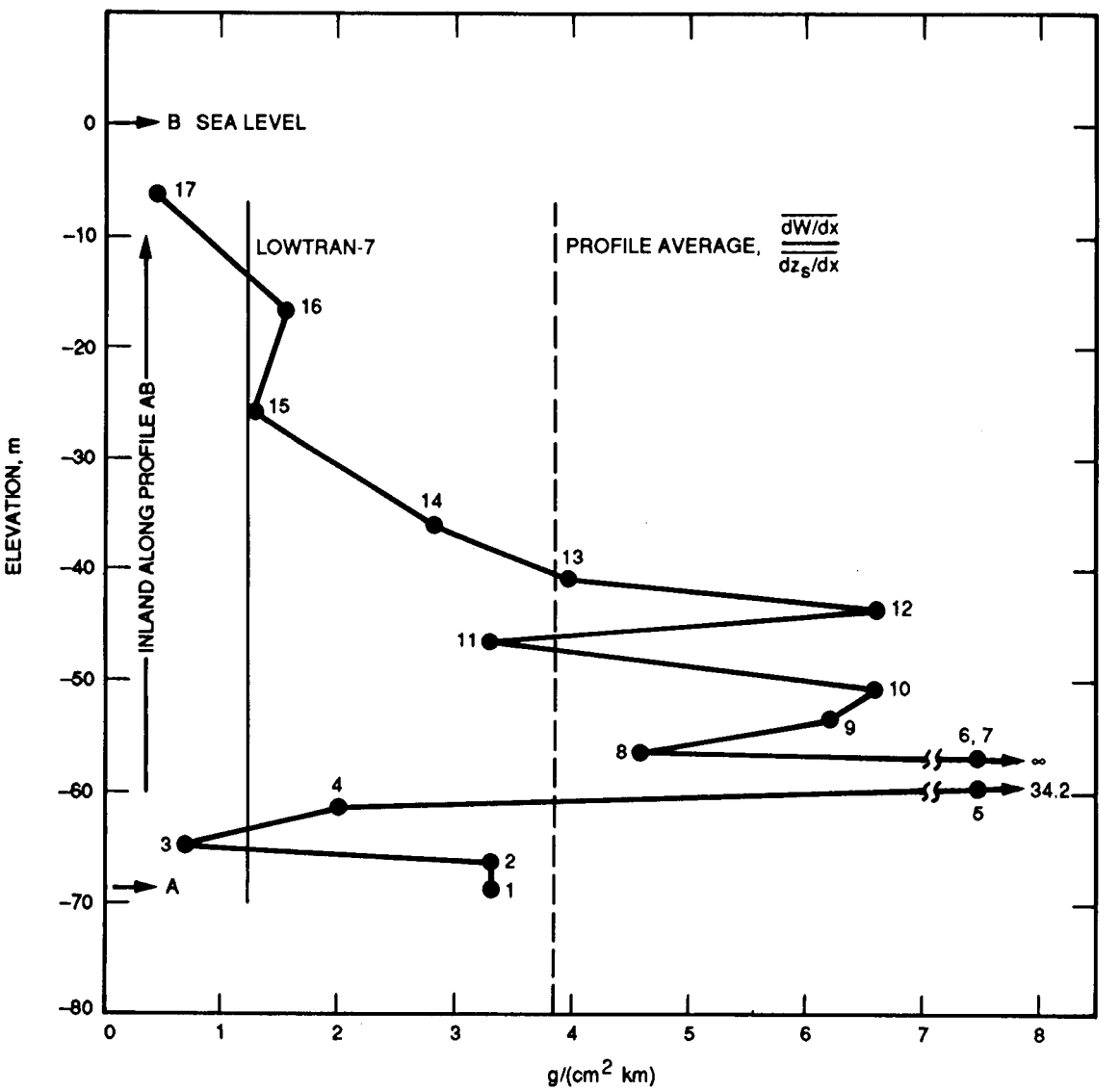

Figure 6. Vertical concentration of water vapor (in g/(cm^{2}km)) over the western shore site implied by the horizontal gradients of moisture and topography in a horizontally stratified atmospheric model. The LOWTRAN 7 vertical distribution was scaled to give observed shoreline precipitable water. The profile average concentration was calculated by averaging derivatives for points along the profile. Numbers on points refer to successive points in the cross section.

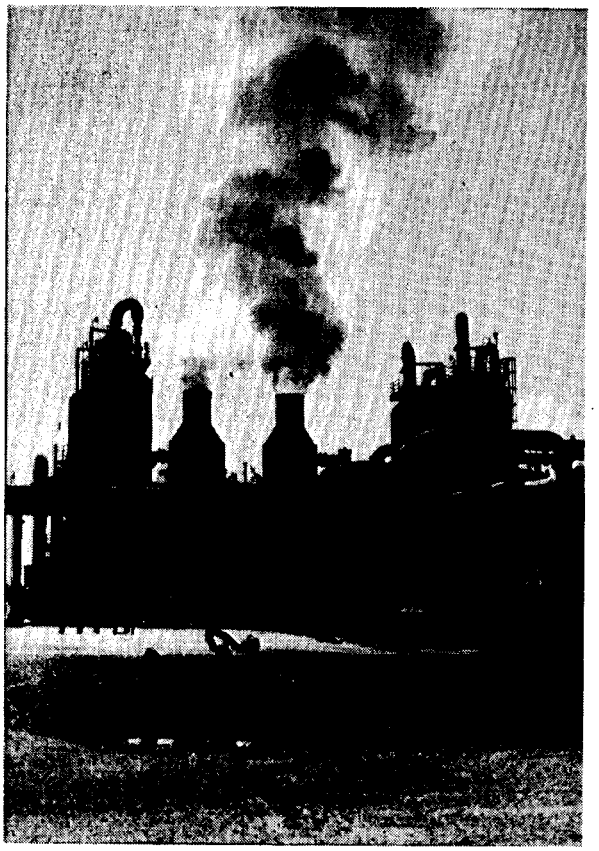

Figure 7. Flash towers at the UNOCAL Unit 3 geothermal power facility, Imperial Valley, CA.

Figure 8. Water vapor column abundance distribution over the southern shoreline and geothermal plant site calculated from the 1130-nm band. A median filter replaces the image DN value at Pixel P with the most frequent value in the 3x3 array with P at the center.

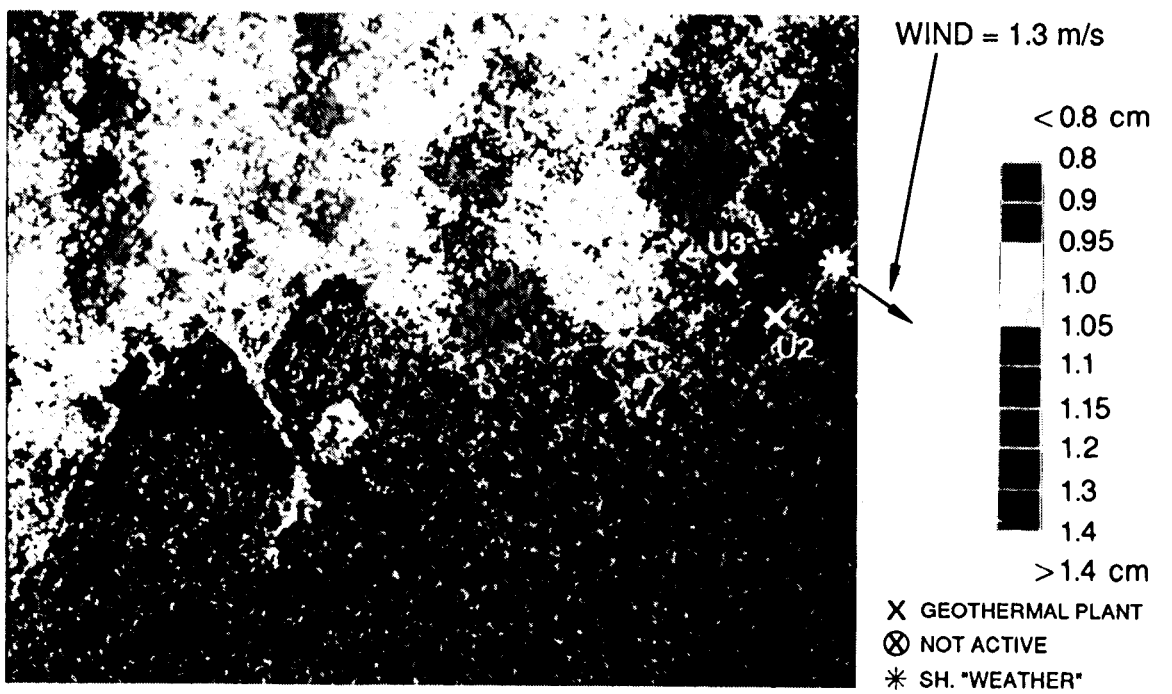

Spatial distribution of water vapor
1130 nm Atmospheric water band
Median Filter

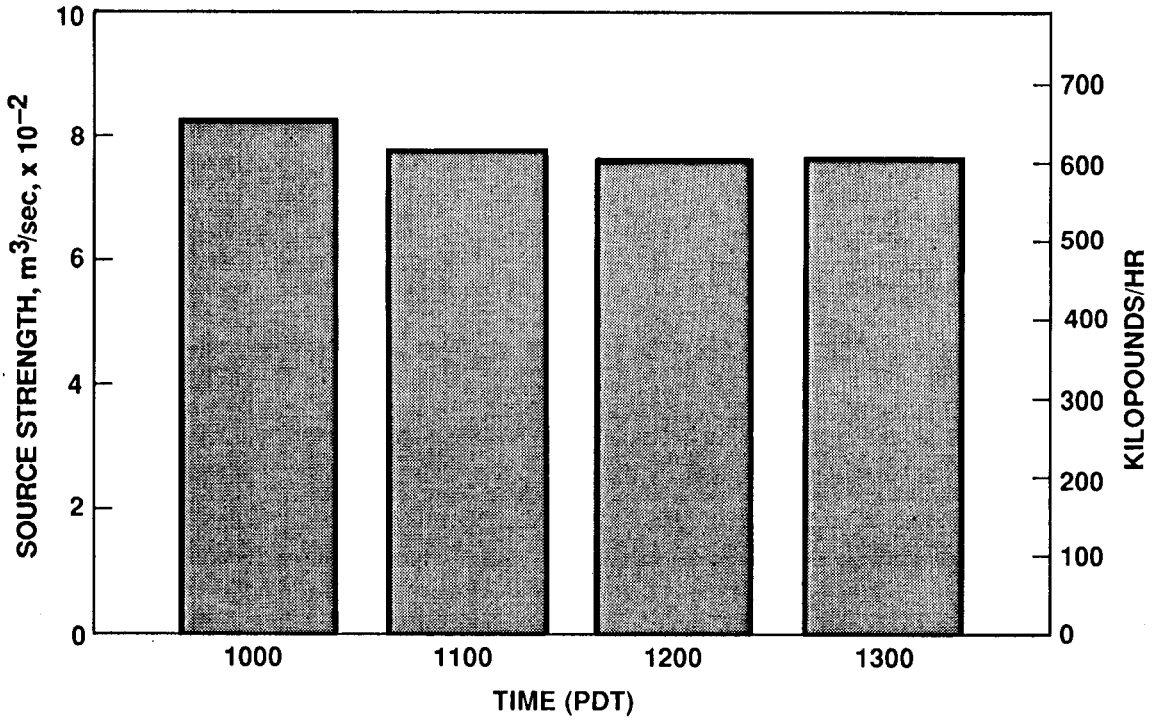

Figure 9. Rate of water loss from the UNOCAL No. 3 Unit cooling evaporators and flash towers for April 18, 1989. AVIRIS overflew the site at 12:10 PDT.

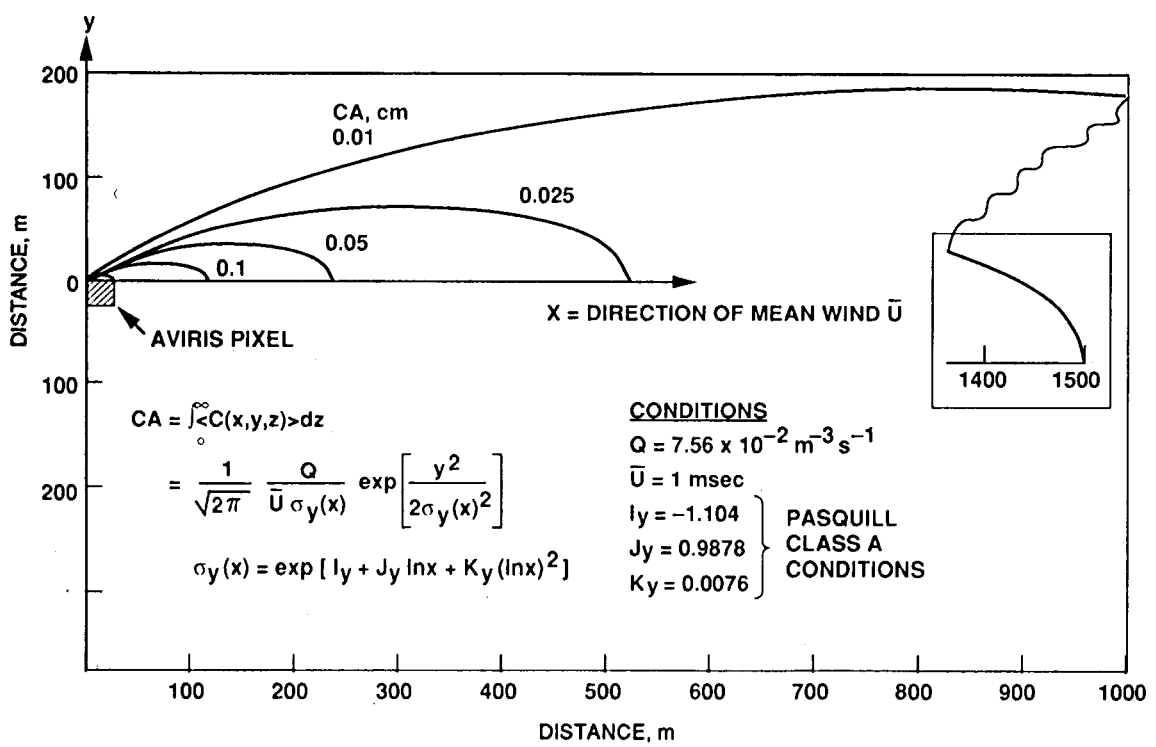

Figure 10. Contours of constant column abundance for a point source in steady horizontal wind and perfectly reflecting (zero absorption) surface. Source strength is that measured for the UNOCAL Unit 3 plant as determined from the data of Figure 9.